

Lab on a Chip

Accepted Manuscript



This is an *Accepted Manuscript*, which has been through the Royal Society of Chemistry peer review process and has been accepted for publication.

Accepted Manuscripts are published online shortly after acceptance, before technical editing, formatting and proof reading. Using this free service, authors can make their results available to the community, in citable form, before we publish the edited article. We will replace this *Accepted Manuscript* with the edited and formatted *Advance Article* as soon as it is available.

You can find more information about *Accepted Manuscripts* in the [Information for Authors](#).

Please note that technical editing may introduce minor changes to the text and/or graphics, which may alter content. The journal's standard [Terms & Conditions](#) and the [Ethical guidelines](#) still apply. In no event shall the Royal Society of Chemistry be held responsible for any errors or omissions in this *Accepted Manuscript* or any consequences arising from the use of any information it contains.

A Microfabricated Optofluidic Ring Resonator for Sensitive, High-Speed Detection of Volatile Organic Compounds

Kee Scholten,^{a,e} Xudong Fan,^{b,e} and Edward T. Zellers^{c-e}*

^aApplied Physics Program, University of Michigan, Ann Arbor, MI, USA 48109-1040

^bDepartment of Biomedical Engineering, University of Michigan, Ann Arbor, MI, 48109-2110

^cDepartment of Environmental Health Sciences, Univ. of Michigan, Ann Arbor, MI, 48109-2029

^dDepartment of Chemistry, University of Michigan, Ann Arbor, MI, 48109-1055

^eCenter for Wireless Integrated MicroSensing and Systems, Univ. of Michigan, Ann Arbor, MI, 48109-2121

*Address correspondence to ezellers@umich.edu

Abstract

Advances in microanalytical systems for multi-vapor determinations to date have been impeded by limitations associated with the microsensor technologies employed. Here we introduce a microfabricated optofluidic ring resonator (μ OFRR) sensor that addresses many of these limitations. The μ OFRR combines vapor sensing and fluidic transport functions in a monolithic microstructure comprising a hollow, vertical SiO_x cylinder (250- μm i.d., 1.2- μm wall thickness; 85- μm height) with a central quasi-toroidal mode-confinement section, grown and partially released from a Si substrate. The device also integrates on-chip fluidic-interconnection and fiber-optic probe alignment features. High-Q whispering gallery modes generated with a tunable 1550-nm laser exhibit rapid, reversible shifts in resonant wavelength arising from polymer swelling and refractive index changes as vapors partition into the \sim 300-nm PDMS film lining the cylinder. Steady-state sensor responses varied in proportion to concentration over a 50-fold range for the five organic vapors tested, providing calculated detection limits as low as 0.5 ppm (v/v) (for m-xylene and ethylbenzene). In dynamic exposure tests, responses to 5- μL injected m-

xylene vapor pulses 710 ms wide were only 18% broader than those from a reference flame-ionization detector and also varied linearly with injected mass; 180 pg was measured and the calculated detection limit was 49 pg without use of preconcentration or split injection, at a flow rate compatible with efficient chromatographic separations. Coupling of this μ OFRR with a micromachined gas chromatographic separation column is demonstrated.

Introduction

Advances in photonics have yielded a new class of sensors adapted from whispering-gallery-mode (WGM) resonators.^{1,2} These devices confine light at resonant wavelengths (λ_{WGM}) determined by the resonator material and dimensions, and the refractive index (RI) of the medium near the waveguide surface. Shifts in λ_{WGM} from changes in the composition of a bulk fluid,^{3,4} binding to surface-immobilized bio-receptors,⁵ or partitioning into a sorptive surface layer,^{6,7} afford label-free, RI-based detection of biological and chemical analytes. The typical sensor configuration comprises a narrow Si ridge in the shape of a loop (i.e., a micro-ring) that is sealed within a flow cell,^{4,5,7} but sensors have also been made from disk⁸ and toroidal⁹ resonators on planar substrates. Although most commonly applied to liquid-phase analyses,^{1,3-5,8,10} brief reports on gas-phase detection of single volatile organic compounds (VOC) with optical micro-ring resonators have also appeared.^{6,7} The latter exhibit rather low sensitivities and long response times. Moreover, no studies of these devices have yet addressed the challenges of efficiently packaging the gas-phase fluidic and sensing components or integrating them into gas chromatographic microsystems (μ GC) suitable for analyzing the trace-level components of complex VOC mixtures encountered in most real-world environmental or clinical applications.

The optofluidic ring resonator (OFRR) is a variant of such sensors that incorporates sensing and fluidic transport features into a single structure.¹¹⁻¹⁴ In such devices, WGMs are excited in the narrowed wall of a dielectric capillary by a coupled external waveguide. The evanescent component of the WGM extends into the fluid filled interior of the OFRR, and changes in RI within the evanescent field at the inner surface cause a shift in λ_{WGM} according to the following expression:¹³ $\Delta\lambda_{WGM} = 2\pi r \Delta n_{eff}/m$, where r is the radius of the OFRR, m is an integer specifying the mode number, and n_{eff} is the effective RI that takes into account of the mode distribution in the air, wall, surface layer and fluid.

The first reported OFRR sensors were fabricated from heat-drawn glass capillaries that were etched to further thin the wall and then lined with sorptive polymer films.¹¹⁻¹³ Shifts in λ_{WGM} would occur from changes in the polymer film thickness and/or RI accompanying reversible partitioning of VOC analytes flowing through the capillary. With Q-factors as high as 10^6 and inner diameters $\leq 100 \mu\text{m}$, such OFRRs could serve as sensitive, stand-alone VOC sensors,¹¹ and as detectors downstream from conventional GC separation columns for the analysis of VOC mixtures.^{12,14} However, such OFRRs are not well-suited for microsystem integration because they are fragile and cumbersome, their diameters and wall thicknesses are difficult to control, and they are not amenable to batch fabrication either as individual sensors or as multi-sensor arrays. The enticing prospect of integrating OFRR detectors into μGC instrumentation demands an alternative design.

Here we introduce a fully functional *microfabricated* optofluidic ring resonator (μOFRR) sensor that addresses the limitations of capillary-based OFRR designs and has performance characteristics rivaling or exceeding those of other microsensors technologies that have been studied as (μ)GC detectors.¹⁵⁻²⁸ Fabricated from Si by batch-scalable micromachining

techniques, the device we describe here integrates a PDMS-coated, 250- μm i.d SiO_x μOFRR cylinder, a microfluidic interconnection channel, capillary insertion port, and an optical-fiber alignment structure on a 4- cm^2 Si chip. A quasi-toroidal expansion contour in the center of the cylinder serves to confine WGMs within a narrow region of the cylinder, thereby increasing sensitivity and reducing the effective sensing volume to ~ 45 pL. This device represents a refinement of μOFRR test structures on which we have reported previously,²⁹ which had cylinder diameters ranging from 50 to 200 μm , wall thicknesses of ~ 2 μm , and Q-factors ranging from 9,200 to 15,000 (comparable to planar Si ring-resonator sensors³⁰); those structures lacked a complete fluidic pathway (i.e., the floor of the cylinder was still intact) and they had not been coated or tested as VOC sensors. Note that this μOFRR differs from recently reported OFRRs produced by strain-induced self-rolling of SiO/SiO₂ bilayers,^{31,32} which have been adapted as on-chip detectors for liquid-phase analytes; with inner diameters of ~ 10 μm and comparatively low Q-factors. Such devices are not suitable for vapor detection or μGC integration.

After briefly describing the key features of the μOFRR chip design and operation, results of vapor-phase calibrations with five common VOCs are presented under steady-state conditions, and relative sensitivities are assessed with respect to the relative contributions of polymer swelling and RI changes. We then demonstrate the rapid responses and low limits of detection (LOD) achievable with the μOFRR sensor under transient exposure conditions, and finally show a high-speed separation of a simple VOC mixture with the μOFRR installed downstream from a μGC column.

Experimental

All test compounds were used as received (99% purity). Relevant physical properties are listed in Table 1. PDMS was obtained from Ohio Valley Specialty Company (OV-1, Marietta,

OH). μ OFRR devices were fabricated from Si by a combination of dry isotropic etching, deep reactive ion etching (DRIE), and thermal oxidation steps, as described previously.²⁹ The DRIE cylindrical resonator extends through the Si substrate. It expands from 250 to 310 μm i.d. in a quasi-toroidal shape along its midsection. Successive oxidation steps reduced surface roughness and a final oxidation grew the SiO_x structure to the desired 1.2 μm thickness. It was partially released from its Si “mold” by an isotropic plasma etch. A DRIE alignment channel runs laterally across the entire 2 \times 2 cm chip and facilitates tangential contact of the thinned optical fiber with the expanded section of the μ OFRR cylinder (see Figure 1).

Fluidic interconnection structures include a tapered DRIE channel ($\sim 380 \times 380 \times 5000$ μm) on the backside of the chip that secures the inserted capillary and conducts gas flow through a microfluidic path ($250 \times 250 \times 5000$ μm) to the backside aperture of the μ OFRR. Following PDMS film deposition (see below), a 2 \times 2 cm Pyrex cover plate was affixed to the backside of the chip with UV-curable adhesive to seal the fluidic channel. A short segment of deactivated fused-silica capillary (250 μm i.d.) was inserted in the channel and sealed with epoxy.

To coat the device (prior to applying the backside cover plate), the sensor chip was inverted and gently pressed into a rubber septum to form a tight seal. Then 10 μL of a 2.3 mg/mL solution of PDMS in toluene was deposited over the backside port. The chip was placed in a vacuum chamber that was evacuated to allow the PDMS solution to fill the resonator cavity. Following evaporation of the solvent a ~ 300 nm layer of PDMS remained on the internal wall of the μ OFRR (assuming uniform deposition). The presence of the film was apparent from the change in the appearance of the resonator expansion section by optical microscopy.

WGM resonances were excited by evanescently coupling to a 1550-nm laser source (CQF939/251, Philips, Amsterdam, NE) sweeping 375 pm at 10 Hz. An unclad section of an

optical fiber (SMF-28, Corning Inc., Corning, NY) was drawn over a flame and tapered to $\sim 1 \mu\text{m}$ o.d.¹¹ The untapered segments of the fiber were glued to a horizontal frame, which was secured to an adjustable stage with a Vernier micrometer, and the tapered segment of the fiber was lowered into the alignment channel in direct contact with the expanded section of the μOFRR cylinder. The proximal end of the fiber was connected to the laser and the distal end of the fiber directed at an IR photoreceiver (Model 2033, New Focus, Irvine, CA). The power required to operate the detection system was very low: the μOFRR sensor is passive, the laser required < 30 mW from a bench scale power supply, and the photoreceiver was operated from a 9V battery.

Each WGM resonance formed a Lorentzian trough in the transmitted intensity; λ_{WGM} was defined as the wavelength of minimum transmission and recorded along with the FWHM value of the resonance. The shift of λ_{WGM} was monitored during VOC exposures. Responses of the μOFRR sensor were recorded for each of five VOCs individually over a 50-fold range of concentration. Test atmospheres were prepared in 3-L Tedlar[®] bags. Concentrations were confirmed by injecting aliquots into a pre-calibrated GC (Model HP-5890, Agilent Technologies, Palo Alto, CA) equipped with a 30-m PDMS-coated capillary column and flame-ionization detector (FID). The minimum concentration ranged from 5 (m-xylene) to 68 (benzene) mg/m^3 (1.2 – 21 ppm). Samples from the test atmosphere were drawn into in a 1-mL sampling loop via a 6-port valve and injected through a 10-cm segment of deactivated fused silica capillary (100- μm i.d.) into the μOFRR sensor in dry air at 3 mL/min. This resulted in exposure times of ~ 20 s, which was sufficient for responses to reach steady state. Five replicates were measured at each of five or six bag concentrations of each VOC. Subsequently, tests with m-xylene were repeated with a 5- μL sample loop (3 mL/min) to evaluate responses to transient exposures.

The μ OFRR sensor was then connected by deactivated capillary to an upstream separation μ column comprising 3.1×3.1 cm Si chip containing a 3-m-long DRIE square-spiral channel with a wall coating of PDMS.^{33,34} The μ column was held at 63 °C using an on-chip resistive heater, and the μ OFRR was at room temperature (~ 22 °C). A test atmosphere containing a mixture of benzene, toluene, n-octane and m-xylene was drawn through the 5- μ L sample loop and injected into the μ column in dry air at 1.4 mL/min. Injected masses ranged from 20 (m-xylene) to 100 (benzene) ng.

Results and discussion

Figure 1a illustrates the features and the operating configuration of this new μ OFRR sensor. Figure 1b shows an SEM image of the μ OFRR with an adjacent optical-fiber probe, prior to PDMS coating application, and Figure 1c shows a photograph of the entire chip with an external capillary affixed to the inlet port. The image shown in Figure 1d is a photomicrograph of the capillary installed in the Pyrex-capped, tapered channel on the backside of the μ OFRR chip.

Figure S1 (ESI†) shows an isolated WGM mode at 1550 nm. The average Q-factor of the uncoated μ OFRR, defined as the ratio of λ_{WGM} to the full-width-at-half-maximum (FWHM) value of each of the resonances, was 11,500. It was unchanged following deposition of the PDMS film, which indicates a negligible optical loss of the mode resulting from PDMS absorption. This Q-factor is lower than those reported for some capillary-based OFRRs, most likely due to residual surface roughness from etching, despite successive oxidation steps intended to reduce such roughness. However, the line-width is sufficiently narrow to resolve small shifts in λ_{WGM} .

All vapor exposures caused red shifts in λ_{WGM} that were completely reversible. A video showing the raw response of the sensor is provided in the ESI†. The rise and fall times for a given vapor exposure were remarkably short in all cases: < 2.5 s and 5.8 s, respectively, to and from steady-state. The lower inset in Figure 2a shows the response profile for 700 mg/m³ (i.e., 190 ppm) of toluene vapor, which is typical of all profiles for the ~20 s exposures employed. Figure 2a presents the individual calibration curves for the five VOCs on the basis of steady-state responses. Replicate responses were highly reproducible (RSD \leq 3%) and all curves were linear ($R^2 > 0.99$, forced zero y-intercept). Calculated slope sensitivities are presented in Table 1.

LODs, defined as $3\sigma/\text{sensitivity}$, where σ (= 0.131 pm) is the standard deviation of the baseline signal, range from 2.2 to 22 mg/m³ (0.51 to 6.9 ppm) among the five VOCs (Table 1). These steady-state LODs are 1-2 orders of magnitude lower than those reported for ethanol (vapor pressure, $p_v = 8.8$ kPa) with a polyethylene glycol coated capillary-based OFRR under similar exposure conditions.¹¹ Although several factors can affect LODs (see below), the thinner wall and mode confinement feature of the μOFRR , which increase the proportion of the WGM evanescently probing the PDMS film, undoubtedly contribute to the higher sensitivity observed.

Thermodynamically, the extent of partitioning into a non-polar polymer such as PDMS should be inversely proportional to the p_v value of the VOC.³⁵ Accordingly, using published values of the partition coefficient, K , in PDMS (Table 1) for the analytes tested here, a plot of p_v vs. K is linear ($r^2 = 0.997$). By regressing sensitivity values (Table 1) onto those published K values, we can explore the extent to which the vapor pressures of the VOCs affect their μOFRR responses. Figure 2b presents such a plot. As shown, the aromatic compounds fall along the same trend line ($r^2 = 0.986$), while the alkane, n-octane, falls well below the line. This indicates

that the relative responses among the aromatic vapors vary in proportion to their p_v values, whereas the relative response to n-octane vapor is affected by other factors.

To better understand this, we can express the response of the μ OFRR as a function of two terms, as follows:¹³

$$\Delta\lambda_{WGM} = \frac{\partial\lambda_{WGM}}{\partial n_{PDMS}} \Delta n_{PDMS} + \frac{\partial\lambda_{WGM}}{\partial t} \Delta t \quad (1)$$

where t is the PDMS film thickness. Assuming that the evanescent field of the WGM extends into the interior beyond the PDMS coating, then $\partial\lambda_{WGM}/\partial t$ would be non-zero, because film swelling would increase the portion of the WGM in the PDMS, which has a higher RI value than that of air, regardless of the RI of the vapor. For operation in such a “thin-film” regime,³⁶ the second (“swelling”) term of Eq. 1 would always be positive, and λ_{WGM} would be red-shifted. Since we know that $\partial\lambda_{WGM}/\partial n_{PDMS}$ is finite and positive, the contribution of the first (“RI-shift”) term of Eq. 1 to the net response depends on the RI value of the vapor relative to that of the PDMS: a vapor with a higher RI will red-shift λ_{WGM} while a vapor with a lower RI will blue-shift λ_{WGM} . In the former case the response due to swelling would be enhanced and in the latter case it would be diminished.

As stated above, red-shifts in λ_{WGM} were observed upon exposure to all vapors. The RI values (Table 1) for the aromatic VOCs are similar (i.e., 1.493-1.501 RIU) and are all greater than that of PDMS (i.e., 1.404 RIU).³⁷ In contrast, the RI of n-octane (i.e., 1.394 RIU) is slightly lower than that of PDMS. Thus, the sensitivities to the aromatic vapors are enhanced to a similar extent over that expected on the basis of swelling alone, whereas the sensitivity to n-octane is unaffected or slightly diminished. It is for this reason that the n-octane sensitivity falls below the trend line in Figure 2b. This also provides presumptive evidence that the device is operating in the thin-film regime.

To quantify the contribution attributable to ΔRI we used the published K values, the absolute air concentrations, and the (liquid) densities of the test compounds to calculate their volume fractions, φ , in the PDMS. Swelling-normalized sensitivity values, in pm/ φ , were then calculated: for n-octane the value is 26,000 pm/ φ and for the aromatic compounds the average value is 68,300 pm/ φ (ratio = 2.6), reflecting the enhancement from ΔRI for the latter compounds.

The relative contributions of swelling and ΔRI to the net response can be estimated via Eq. 1. Assuming that $\partial\lambda_{WGM}/\partial t$ and $\partial\lambda_{WGM}/\partial n_{PDMS}$ are constant over the range of φ values considered, then $\partial\lambda_{WGM}/\partial n_{PDMS} = 416,000$ pm/RIU and $\partial\lambda_{WGM}/\partial t = 101$ pm/nm. For a sorbed vapor with an RI value that is, say, 0.1 RIU greater than that of PDMS, the RI-shift term will be 1.4 times the swelling term in Eq. 1. For the range of RI values spanned by most VOCs, i.e., from 1.35 to 1.55,³⁸ a red shift in λ_{WGM} is predicted in all cases for this PDMS-coated $\mu OFRR$, as observed. Although these results are unique to the specific film thickness considered here, they highlight that the $\mu OFRR$ is both a volumetric and refractometric sensor, and that sensitivity and selectivity depend on both the K value and the contrast between the RI values of the VOC and the selected sorbent.

To characterize the $\mu OFRR$ response under transient exposure conditions, a second calibration was performed with m-xylene using 5- μL (loop) vapor injections of a series of test atmospheres into an air carrier gas flowing at 3 mL/min through the sensor. This flow rate is typical of those used for μGC analyses. Both peak height and peak area varied linearly with injected mass over the range tested (i.e., 0.18 to 5.3 ng). The inset of Figure 3 shows the peak-height calibration curve ($R^2 = 0.997$). The calculated sensitivity for m-xylene under these conditions is 23% of that obtained from the steady-state calibration, reflecting the degree to

which sorption fell short of the equilibrium value under these dynamic exposure conditions. In spite of this, an LOD of 49 pg was calculated using the peak-height sensitivity value. This μ OFRR LOD is \sim 100 times lower than that reported for n-decane (i.e., 4.5 ng) with a polymer-coated capillary-based OFRR installed as an in-line detector,¹² despite the use of a split injection and a relatively high flow rate for the n-decane analysis (note: m-xylene was not tested in that study).

In comparing performance among different types of sensors used as GC or μ GC detectors, it must be recognized that the LOD, which is calculated on the basis of peak height, depends as much on system operating parameters and vapor properties as it does on the inherent sensor response characteristics. Kinetic and thermodynamic factors are both important. Among structurally similar compounds, those with lower vapor pressures always have larger K values in sorptive sensor-interface films, leading to higher sensitivities and lower LODs, all other factors being equal. Affinity also affects K values and is determined by the compatibility of the respective functional groups of the analyte and the interface material. However, lower vapor pressures and stronger vapor-interface interactions also reduce the rate of desorption from the interface film, which tends to broaden peaks and raise the LOD. The length of time an analyte spends on the upstream separation (μ)column is also important, as peaks invariably broaden with increasing retention time. Of course, the injection bandwidth is yet another critical factor, with sharper injections leading to taller peaks and lower LODs. This is one reason why split injections are often used to evaluate sensor sensitivities.^{20, 24-26} Although a large fraction of injected sample mass is lost (vented) by use of a high injection split ratio, the injection band becomes very sharp and the *concentration* of the injected sample is (ideally) unaffected, which can provide a significant enhancement in peak-height sensitivity and a commensurate reduction

in the apparent LOD. The effects of temperature and flow rate on the factors presented above can also be significant.^{21,28,39}

The LOD we calculated for m-xylene with the μ OFRR above is 1-3 orders of magnitude lower than those of chemiresistor or surface-acoustic-wave microsensors employing sorptive nanoparticle or polymer interface layers that have been used as portable GC or μ GC detectors under similar operating conditions;^{16, 17, 21, 40, 41} reported LODs were in the range of 0.5-14 ng for m-xylene, though for peaks that were wider than those measured here by virtue of having been injected from an adsorbent preconcentrator and/or separated on an upstream (μ)column. The Fabry-Perot (FP) sensors explored as (μ)GC detectors by Reddy, et al.,²⁴⁻²⁶ were not tested with m-xylene, but an LOD of 200 pg for toluene was obtained by probing a PDMS film under conditions that gave a relatively broad toluene peak (i.e., FWHM \approx 1 s).²⁴ The toluene LOD was reduced by as much as \sim 20-fold in subsequent studies by use of a split injector providing nominal split ratios up to 10^4 :1 to decrease the peak width significantly, while maintaining the relatively high flow rate (i.e., 8 mL/min) used in the earlier study.²⁴⁻²⁶ μ GC separations performed at lower flow rates with splitless injection, however, gave broader peaks and consequent reductions in the FP-sensor S/N ratios.²⁶

Thus, although only rough comparisons are possible, the available data suggest that the LOD achievable with our PDMS-coated μ OFRR may be considerably lower than those of other microsensors used as (μ)GC detectors under typical operating conditions. Since the μ OFRR sensitivity varies with the fraction of the WGM in the PDMS film, a reduction in the LOD could be achieved ostensibly by either increasing the thickness of the PDMS film or decreasing the wall thickness of the μ OFRR. However, increases in the PDMS film thickness might also lead to peak broadening due to slower sorption/desorption rates, and would reduce the component of the

response attributable to film swelling (*vide supra*). The SiO_x wall thickness could be reduced with the fabrication method employed here, but this might compromise the structural integrity of the device, and it could also increase baseline noise and decrease the Q-factor.¹³ We speculate that any reductions in LOD realized by such changes in device design would be marginal.

The widths of the peaks for m-xylene from the μOFRR sensor here were limited by the injection volume and flow rate; a splitless injection of 5 μL at 3 mL/min was employed. For reference, analyses were repeated under identical separation conditions with an FID installed in place of the μOFRR . The FID is considered to have ‘zero’ dead time and to serve as an ideal reference for assessing detector band broadening. Figure 3 shows the response profile for a 180-pg injection of m-xylene, and that for a larger injection (~500 pg) of m-xylene from the FID, where the latter profile has been scaled to the same peak height as the former (note: for reference, 180 pg would correspond to a 0.1-L pre-concentrated air sample containing 40 parts-per-billion of m-xylene). As shown, the peak from the μOFRR (FWHM = 0.71 s) is just 18% broader than that from the FID (FWHM = 0.60 s).

This performance is consistent with that reported in other studies where reference FID responses were also collected; peaks from microsensors are invariably wider than the corresponding peaks from an FID due to the finite vapor sorption/desorption rates in microsensor interface films.^{12,15,18,20,40,42,43} Accordingly, the difference in FWHM values increases as the vapor pressure of the analyte decreases.^{12,43} Although the fidelity of the FWHM value of the μOFRR peak to that of the FID for such a narrow peak is noteworthy, it is not unprecedented (see, for example, refs. 12 and 20; also see below), and, generally speaking, will depend on most of the same factors affecting determinations of LODs discussed above. Regardless, this demonstrates that the μOFRR has a very low effective dead volume and a rapid response, which

are certainly important attributes for use in μ GC systems, but perhaps even more important for use in μ GC \times μ GC systems,^{4,45} where very narrow modulated peaks are produced and extra-column sources of band broadening must be strictly minimized. Further reductions in response time should be possible by decreasing the PDMS film thickness or the diameter of the μ OFRR, but with commensurate reductions in sensitivity or increases in flow resistance, respectively.

The chromatogram shown in Figure 4 is an isothermal separation of four of the VOCs obtained with a microfabricated GC column chip coupled to the μ OFRR sensor using dry air as the carrier gas at 1.4 mL/min. This is the first instance of an OFRR sensor used as the detector for a μ GC separation. The VOCs are easily separated in 36 s and the peaks are symmetric and sharp (FWHM = 0.33 to 1.17 s), indicative of excellent response dynamics from the sensor. It is clear from the time required for elution of the first peak (i.e., benzene) that the separation could be accelerated by use of temperature programming, a shorter μ column, or a higher flow rate.

Conclusions

In summary, the μ OFRR is a new microsensor with several attributes that augur well for its use in micro-analytical systems for trace-level VOC determinations. Compared to capillary-based OFRRs, the μ OFRR design reduces the size, increases structural integrity, affords precise control of resonator dimensions, and, by virtue of better mode confinement and thinner walls, yields higher sensitivity. The integration of on-chip microfluidics and fiber alignment structures in the device described here minimizes the dead-space along the flow path and facilitates system integration and packaging. Responses are consistent with theory and, as shown, can be parsed into contributions from swelling and RI changes of the polymer interface films upon reversible vapor sorption. The high sensitivity and rapid response time permits the detection of peaks < 1 s

wide containing pg quantities of vapor at flow rates compatible with efficient chromatographic separations, which is unprecedented. These features will facilitate advancements in high-speed μGC and $\mu\text{GC}\times\mu\text{GC}$ systems for complex VOC analyses. Arrays of such sensors, lined with different sorptive interface materials and integrated on a common Si substrate, can be envisioned. The resulting response patterns produced by the eluting vapors would enhance the reliability of VOC determinations.^{16,17,22,25-27,46} In on-going work we are pursuing the construction of such arrays. We have also assembled a compact module comprising a small laser, a diode detector, and a μOFRR sensor with the fiber probe and capillary interconnect securely fixed in position, which we plan to use in tests with our latest μGC and $\mu\text{GC}\times\mu\text{GC}$ prototypes.

Acknowledgments

The authors express their heartfelt appreciation to Mr. Will Collin for assistance with calibrations, μGC column preparation, and helpful discussions. This work was supported by NSF Grant ECCS 1128157. Devices were fabricated in the Lurie Nanofabrication Facility, a member of the National Nanotechnology Infrastructure Network, which is supported by the NSF.

Footnote

† Electronic supplementary information (ESI) available: Figure S1 showing WGM of coated μOFRR at 1550 nm. Video S1 showing λ_{WGM} shift due to VOC exposure. See DOI: XXX

References

1. F. Vollmer, and S. Arnold, *Nat. Methods*, 2008, **5**, 591-596.
2. X. Fan, I.M. White, S.I. Shopova, H. Zhu, J.D. Suter, and Y. Sun, *Anal. Chim. Acta*, 2008, **620**, 8-26.
3. I.M. White, H. Zhu, J.D. Suter, N.M. Hanumegowda, H. Oveys, M. Zourob, and X. Fan, *IEEE Sens. J.*, 2007, **7**, 28-35.
4. J. Wang and D. Dai, *Opt. Lett.*, 2010, **35**, 4229-4231.
5. A.L. Washburn, L.C. Gunn, and R.C. Bailey, *Anal. Chem.*, 2009, **81**, 9499-9506.
6. A. Ksendzov, M.L. Homer, and A.M. Manfreda, *Electron. Lett.*, 2004, **40**, 63-65.
7. N.A. Yebo, P. Lommens, Z. Hens, and R. Baets, *Opt. Express*, 2010, **18**, 11859-11866.
8. E. Krioukov, D.J.W. Klunder, A. Driessen, J. Greve, and C. Otto, *Opt. Lett.*, 2002, **27**, 512-514.
9. J. Zhu, S.K. Ozdemir, Y.F. Xiao, L. Li, L. He, D.R. Chen, and L. Yang, *Nature Photon.*, 2009, **4**, 46-49.
10. J.H. Wade, and R.C. Bailey, *Anal. Chem.*, 2014, **86**, 913-919.
11. Y. Sun, S.I. Shopova, G. Frye-Mason, and X. Fan, *Opt. Lett.*, 2008, **33**, 788-790.
12. S.I. Shopova, I.M. White, Y. Sun, H. Zhu, X. Fan, G. Frye-Mason, A. Thompsons, and S.J. Ja, *Anal. Chem.*, 2008, **80**, 2232-2238.
13. Y. Sun and X. Fan, *Opt. Express*, 2008, **16**, 10254-10268.
14. Y. Sun, J. Liu, D.J. Howard, G. Frye-Mason, A.K. Thompson, S. J. Ja, and X. Fan, *Analyst*, 2010, **135**, 165-171.
15. Q.Y. Cai, and E.T. Zellers, *Anal. Chem.*, 2002, **74**, 3533-3539.
16. C.J.Lu, J. Whiting, R. D. Sacks, and E.T. Zellers, *Anal. Chem.*, 2003, **75**, 1400-1409.
17. C.J. Lu, W. H. Steinecker, W-C. Tian, M. Oborny, J. Nichols, M. Agah, J. Potkay, H. Chan, J. Driscoll, R.D. Sacks, K. Wise, S. Pang, and E.T. Zellers, *Lab Chip*, 2005, **5**, 1123-1131.
18. C.Y. Lee, R. Sharma, A.D. Radadia, R.I. Masel, and M.S. Strano, *Angew. Chem. Int. Ed.*, 2008, **47**, 5018-5021.

19. S. Zampolli, I. Elmi, F. Mancarella, P. Betti, E. Dalcanale, G. C. Cardinali, and M. Severi, *Sens. Act. B, Chem*, 2009, **14**, 322-328.
20. M. Li, E.B. Myers, H.X. Tang, S.J. Aldridge, H.C. McCaig, J.J. Whiting, R.J. Simonson, N.S. Lewis, and M.L. Roukes, *Nano Letters*, 2010, **10**, 3899-3903.
21. Q. Zhong, W.H. Steinecker, and E.T. Zellers, *Analyst*, 2009, **134**, 283-293.
22. S.K. Kim, H. Chang, and E.T. Zellers, *Anal. Chem.*, 2011, **83**, 7198-7206.
23. S. Narayanan, B. Alfeeli, and M. Agah, *IEEE Sens. J.*, 2012, **12**, 1893-1900.
24. K. Reddy, Y. Guo, J. Liu, W. Lee, M.K. Khaing Oo, and X. Fan, *Sens. Act. B, Chem.*, 2011, **159**, 60-65.
25. K. Reddy, Y. Guo, J. Liu, W. Lee, M.K. Khaing Oo, and X. Fan, *Lab Chip*, 2012, **12**, 901-905.
26. K. Reddy, J. Liu, M.K. Khaing Oo, and X. Fan, *J. MEMS*, 2013, **22**, 1174-1179.
27. W. R. Collin, G. Serrano, L. K. Wright, H. Chang, N. Nuñoovero, and E. T. Zellers, *Anal. Chem.*, 2014, **86**, 655-663.
28. R.S. Jian, R. X. Huang, and C. J. Lu, *Talanta*, 2012, **88**, 160-167.
29. K. Scholten, X. Fan and E. T. Zellers, *Appl. Phys. Lett.*, 2011, **99**, 141108-141108.
30. M. Zourob, and A. Lakhtakia. *Optical Guided-wave Chemical and Biosensors II: II* (Vol. 2). Heidelberg , Springer, 2010.
31. G. Huang, V. A. B. Quiñones, F. Ding, S. Kiravittaya, Y. Mei, and O. G. Schmidt, *ACS Nano*, 2010, **4**, 3123-3130.
32. S. M. Harazim, V. A. B. Quiñones, S. Kiravittaya, S. Sanchez, and O.G. Schmidt, *Lab Chip*, 2012, **12**, 2649-2655f.
33. S. Reidy, D. George, M. Agah, and R. Sacks, *Anal. Chem.*, 2007, **79**, 2911-2917.
34. G. Serrano, S. M. Reidy, and E. T. Zellers, *Sens. Act. B, Chem.*, 2009, **141**, 217-226.
35. A. Hierlemann, A. J. Ricco, K. Bodenhöfer, A. Dominik, and W. Göpel, *Anal. Chem.*, 2000, **72**, 3696-3708.
36. A. M. Kummer, A. Hierlemann, and H. Baltes, *Anal. Chem.*, 2004, **76**, 2470-2477.

37. Ohio Valley Specialty Company, (2014, February 24). [Online]. Available: <http://www.ovsc.com/>.
38. *CRC Handbook of Chemistry and Physics*, ed. D. R. Lide, CRC Press, Boca Raton, USA, 94th edn., 2013.
39. L. Wright and E. T. Zellers, *Analyst.*, 2013, **138**, 6860-6868.
40. C. J. Lu and E. T. Zellers, *Anal. Chem.*, 2001, **73**, 3449-3457.
41. C.-J. Lu, C. Jin, and E. T. Zellers, *J. Environ. Monit.*, 2006, **8**, 270-278.
42. W. H. Steinecker, M. P. Rowe, A. J. Matzger, and E. T. Zellers, *Proceedings of the 12th International Conference on Solid-State Sensors, Actuators and Microsystems -- Transducers '03*, Boston, MA, June 8-12, 2003, 1343-1346.
43. C.J. Lu, and E.T. Zellers, *Analyst*, 2002, **127** 1061-1068.
44. G. Serrano, D. Paul, S. J. Kim, K. Kurabayashi, and E. T. Zellers, *Anal. Chem.*, 2012, **84**, 6973-6980.
45. W. Collin, A. Bondy, D. Paul, K. Kurabayashi, and E.T. Zellers, *in final preparation*.
46. M. D. Hsieh and E. T. Zellers, *Anal. Chem.* 2004, **76**, 1885-1895.
47. P.J. Linstrom and W.G. Mallard, Eds., NIST Chemistry WebBook, NIST Standard Reference Database Number 69, National Institute of Standards and Technology, Gaithersburg, MD, <http://webbook.nist.gov>, (retrieved January 6, 2014).
48. P. A. Martos, A. Saraullo, and J. Pawliszyn, *Anal. Chem.*, 1997, **69**, 402-408.

Table 1 Physical properties and steady-state sensor response parameters for all VOC analytes.^a

VOC	RI ^b	ρ (g/ml) ^b	p_v (kPa) ^c	K_{PDMS} ^d	Sensitivity (pm/(mg/m ³))	LOD (mg/m ³ :ppm)
benzene	1.501	0.877	12.0	296	0.018	22:6.9
toluene	1.494	0.867	3.78	817	0.070	5.6:1.5
ethylbenzene	1.493	0.867	1.25	2020	0.181	2.2:0.51
m-xylene	1.494	0.860	1.10	2190	0.174	2.3:0.53
n-octane	1.394	0.703	1.71	1486	0.055	7.2:1.5

^a refractive index (RI), density (ρ), vapor pressure (p_v) and partition

coefficient (K) values at 25 °C; ^b ref. 38; ^c ref. 47; ^d ref.48

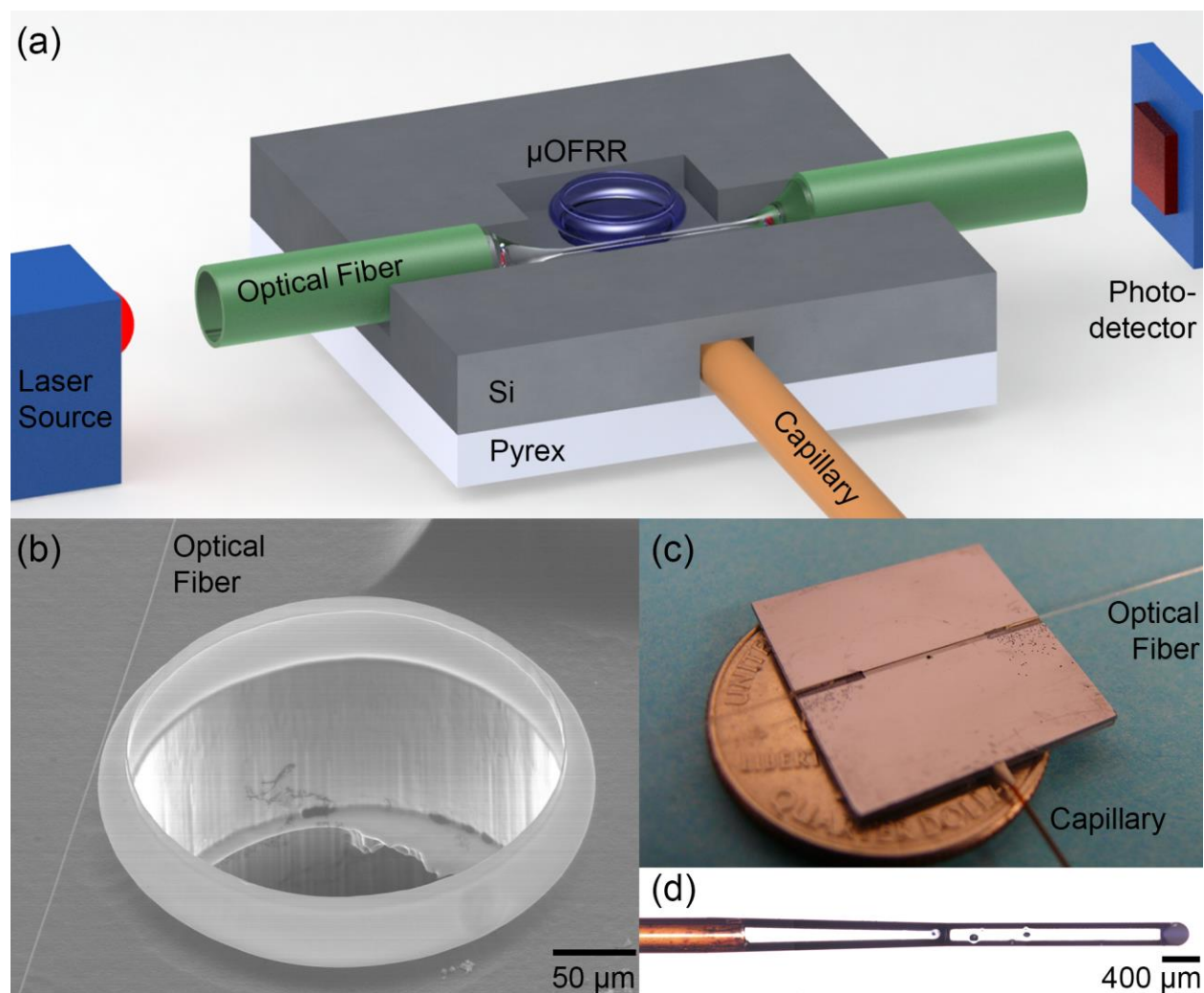


Fig. 1 μ OFRR sensor (a) Illustration depicting the μ OFRR sensor in its operating configuration. (b) SEM image of μ OFRR with tapered fiber (left) in contact with the toroidal expansion section. (c) Photograph of the μ OFRR sensor chip with a fiber waveguide in the alignment channel and a capillary in the fluidic interconnection port. (d) Backside image of the μ OFRR sensor chip showing a capillary (amber color to the left) inserted into the Pyrex-sealed fluidic interconnection channel leading to the μ OFRR inlet port to the right.

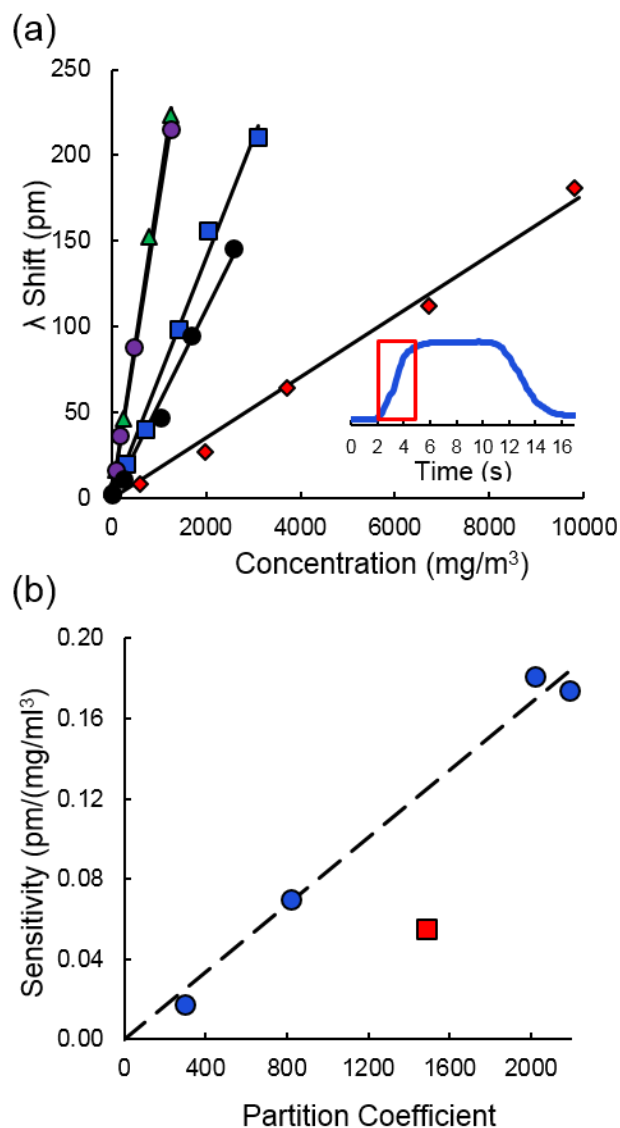


Fig. 2 PDMS-lined μ OFRR sensor responses to steady-state exposures. (a) Calibration curves for benzene (diamond), toluene (square), ethylbenzene (triangle), m-xylene (filled circle), and n-octane (unfilled circle) vapors. Each data point represents the average of 5 replicates. Inset shows the response profile to 700 mg/m³ (190 ppm) of toluene; red square shows a rise time of less than 2.5 s. (b) Sensitivities of benzene, toluene, ethylbenzene and m-xylene (BTEX, blue circles) and n-octane (red square) as a function of their respective partition coefficients, K (Table 1). Trend line shows linear regression for the BTEX analytes.

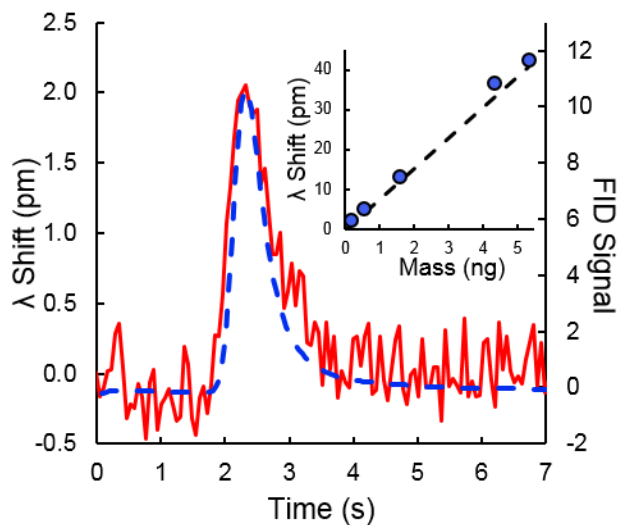


Fig. 3. Rapid response of the μ OFRR to transient VOC exposure. Response profiles from the μ OFRR (solid red line, left axis) for a 180-pg injection of m-xylene vapor and the FID (dashed blue line, right axis) for a \sim 500-pg injection of m-xylene vapor under the same analytical conditions. The FID profile has been scaled down to match the peak maximum from the μ OFRR for comparison of the FWHM values, which were 710 (μ OFRR) and 600 ms (FID). Inset shows the μ OFRR calibration curve for m-xylene from a series of similar injections at higher vapor concentrations.

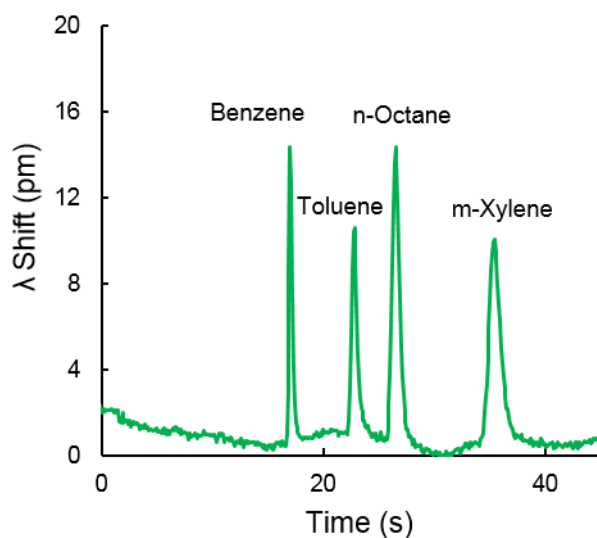
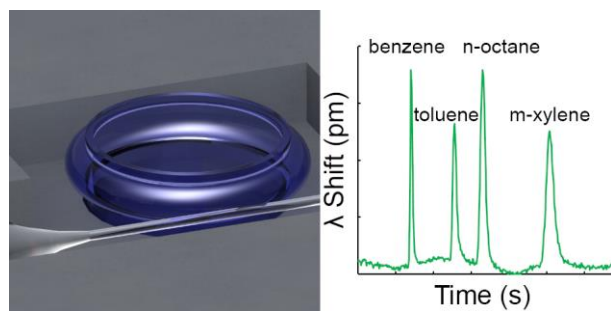


Fig. 4 μ GC separation with μ OFRR sensor as detector. Separation of benzene, toluene, n-octane and m-xylene using a 3.1×3.1 cm μ column chip containing a 3-m long PDMS-coated channel at 63 °C and the (downstream) μ OFRR sensor at 22 °C. Injected masses were approximately 53 ng (benzene), 21 ng toluene, 26 ng (n-octane), and 11 ng (m-xylene). Dry air at 1.4 mL/min was used as carrier gas.

Table of Contents



A microfabricated optofluidic ring resonator (μ OFRR) sensor is introduced and its utility as a detector for micro-scale gas chromatography is assessed.